Dalton Transactions

ROYAL SOCIETY OF CHEMISTRY

PAPER

View Article Online
View Journal | View Issue

Cite this: *Dalton Trans.*, 2026, **55**, 1234

Gold(I) alkoxide and thiolate complexes as potential atomic layer deposition precursors

Nicholas A. Hoffman and David J. H. Emslie *

Reactions of $AuCl(PR_3)$ with $NaOC(CF_3)_3$ in the presence of 1 equiv. of $Ag[BF_4]$ or $Ag[PF_6]$ afforded the gold(I) alkoxide complexes $[(Au\{OC(CF_3)_3\}(PR_3))_n]$ (R = Me (**1**), Et (**2**), ^{i}Pr (**3**) and ^{t}Bu (**4**)). In our hands, analogous reactions using NaO^tBu (for R = ^{i}Pr) did not yield a thermally robust product. However, the thiolate complexes $[\{Au(S^tBu)(PR_3)\}_n]$ (R = Me (**5**) and ^{i}Pr (**6**)) were accessed by reaction of $[\{Au(S^tBu)\}_n]$ with PR_3. Compound **1** is a trimer featuring linear $Au\{OC(CF_3)_3\}(PMe_3)$ units connected through unsupported aurophilic interactions, whereas more sterically hindered **3** and **4** are monomers in the solid state. Compound **5** is a dimer connected *via* an aurophilic interaction, while **6** is a monomer. In solution, **1** and **3** reacted almost instantly with HBpin or H_3SiPh to afford metallic gold and volatile byproducts (free PR_3 and H_2 accompanied by $\{(F_3C)_3CO\}Bpin$ or a mixture of $\{(F_3C)_3CO\}SiH_2Ph$ and $\{(F_3C)_3CO\}_2SiHPh$). By contrast, analogous reactions with thiolate complex **5** required over 24 hours to reach completion. Complexes **1–4** melted at 105–106, 19–21, 59–61 and 181–183 °C, respectively, and sublimed cleanly between 50 and 80 °C at 5 mTorr. By contrast, **5–6** decomposed (completely or partially) during attempted sublimation at 5 mTorr; in the case of **5**, decomposition was shown to occur *via* phosphine dissociation to re-form $[\{Au(S^tBu)\}_n]$. Of the complexes in this work, **3** offers the best combination of thermal stability and volatility, and the relatively low melting point is attractive. However, **3** was ~4% decomposed after 72 h at 85 °C, and ~10% decomposed after 96 h at 100 °C, forming soluble $[Au(P^iPr_3)_2][H\{OC(CF_3)_3\}_2]$ (**7**), gold metal, and other insoluble product(s). Preliminary ALD reactor experiments using **3** (with a delivery temperature of 85 °C) and HBpin showed gold deposition at 124 °C, and no deposition was observed at this temperature using **3** without HBpin.

Received 27th November 2025,
Accepted 15th December 2025

DOI: 10.1039/d5dt02836a

rsc.li/dalton

Introduction

Thin gold films have high conductivity (2.21 μΩ cm for bulk Au),[1] can exhibit surface plasmon resonance at wavelengths relevant to sensing applications, and are exceptionally resistant to oxidation, leading to a range of applications in photonic and microelectronic devices, including as electrical contacts and interconnects, chemical/biological sensors, and anticorrosion coatings.[2–6] Various techniques can be used to deposit thin (*e.g.* <100 nm) metal films, and of these, Atomic Layer Deposition (ALD) can provide access to films with unparalleled thickness uniformity and conformality, making it essential for microelectronic and photonic device fabrication, especially for deposition on high-aspect ratio substrates.[7,8]

ALD relies upon self-limiting surface-based reactions between a precursor molecule and a co-reactant, which are delivered sequentially to the surface of a substrate in the vapour phase, separated by inert gas purge steps. The precursor molecule typically contains the most electropositive element to be deposited (*e.g.* the metal in a metal-containing film), whereas the co-reactant is selected to react with the precursor to deposit the desired material (*e.g.* metal *vs.* metal oxide *vs.* metal nitride). Precursors for ALD should be thermally robust and volatile at the delivery temperature, to ensure adequate vapour pressure and to prevent decomposition (on a timescale of weeks or months) within the delivery vessel. An ALD precursor must also be thermally stable at the deposition temperature (to prevent thermal decomposition leading to Chemical Vapour Deposition (CVD)) and engage in rapid surface-based reactivity with the co-reactant to afford the target material.[9–12] Liquid or low-melting precursors are also preferable from a practical perspective.[13,14]

ALD processes for metallic gold have been reported using (i) $[AuMe_2(\kappa^2\text{-}S_2CNEt_2)]$ with O_3,[15] (ii) $[AuMe_2\{\kappa^2\text{-}S_2P(O^iPr)_2\}]$ with O_3,[16] (iii) $[AuCl(PEt_3)]$ with 1,4-bis(trimethylgermyl)-1,4-dihydropyrazine $\{(Me_3Ge)_2DHP\}$,[3] (iv) $[AuMe_3(PMe_3)]$ with hydrogen plasma,[17] and (v) $[AuMe_3(PMe_3)]$ with (sequentially) oxygen plasma then H_2O[18] (see **A–D** in Fig. 1 for the structures of the gold precursors). Non-self-limiting deposition of Au thin films has also been described using sequential pulses of [Au{N

Department of Chemistry, McMaster University, 1280 Main St West, Hamilton, Ontario, L8S 4M1, Canada. E-mail: emslied@mcmaster.ca

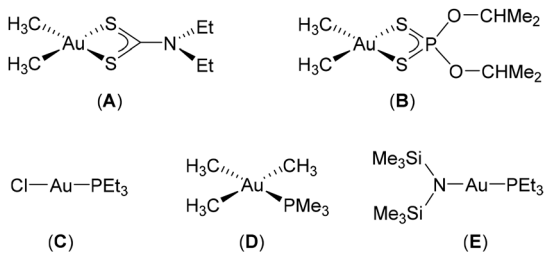

Fig. 1 Gold precursor complexes used for gold deposition *via* ALD or an ALD-like process: **(A)** $[AuMe_2(\kappa^2\text{-}S_2CNEt_2)]$,[15] **(B)** $[AuMe_2\{\kappa^2\text{-}S_2P(O^iPr)_2\}]$[16] **(C)** $[AuCl(PEt_3)]$[3] (the solid state structure consists of 1D chains of $AuCl(PEt_3)$ units with long Au–Au distances),[21] **(D)** $[AuMe_3(PMe_3)]$,[17,18] and **(E)** $[Au\{N(SiMe_3)_2\}(PEt_3)]$.[19]

$(SiMe_3)_2\}(PEt_3)]$ (**E** in Fig. 1) and $BH_3(NHMe_2)$,[19] and Au nanoparticle deposition was achieved using $[AuMe_3(PMe_3)]$ followed by O_3 and then H_2O.[20] Precursors **A**, **B** and **D** in Fig. 1 are square planar gold(III) methyl complexes, whereas **C** and **E** are gold(I) complexes with a linear coordination geometry (the solid state structure of **C** consists of 1D chains of $AuCl(PEt_3)$ units with long Au–Au distances of 3.57–3.62 Å).[21]

Processes i–iii are examples of thermal ALD, where the co-reactant (O_3 or $(Me_3Ge)_2DHP$) is not plasma-generated. By contrast, processes iv–v use plasma-generated hydrogen or oxygen radicals, and are examples of plasma-enhanced ALD (PEALD); PEALD can enable ALD at low temperature and generate films with low impurity content, but increases reactor cost and complexity, is not easily compatible with batch processing, can cause substrate damage, and struggles to achieve conformal metal deposition within high aspect-ratio features (due to rapid recombination of radicals on metal surfaces).[22,23] Processes i, ii and v also use highly oxidizing O_3 or oxygen plasma as the co-reactant, which are incompatible with many substrates, and the minimum deposition temperature for process iii is limited by the volatility of the $[AuCl(PEt_3)]$ precursor (delivered at 160 °C). Thus, the development of gold precursors which offer increased reactivity, thermal stability and/or volatility relative to those currently available, as well as the development of new reaction chemistries which might facilitate gold deposition at lower temperature under non-oxidizing conditions, would be of value.

In this work, we describe linear gold(I) alkoxide ($OC(CF_3)_3$; perfluoro-*tert*-butoxide) and thiolate (*tert*-butylthiolate) complexes with trialkylphosphine neutral donors. Their solution reactivity with potential ALD co-reactants (HBpin and H_3SiPh; pin = $OCMe_2CMe_2O$) and thermal properties (thermal stability, volatility and melting points) are also described, along with preliminary thin film deposition experiments.

Gold(I) alkoxide complexes were targeted in this work due to anticipated high reactivity stemming from the mismatch between hard alkoxide ligands and a soft gold(I) centre;[24–26] the aversion of gold(I) towards hard oxygen donors (and the strong preference of gold(I) to adopt a linear coordination geometry) is well illustrated by the structures of gold(I) acetylacetonate ($CH\{C(O)R\}_2$) complexes, in which the acetylacetonate ligand is κ^1C-coordinated[27–29] rather than adopting a typical κ^2O_2-coordination mode (an X-ray crystal structure of $[Au(\kappa^1C\text{-hfac})(P^iPr_3)]$ (hfac = hexafluoroacetylacetonate = $CH\{C(O)CF_3\}_2$) is provided in Fig. S34). Alkoxides without H or F substituents in the β-position were employed in this work to avoid the potential for β-hydride or β-fluoride elimination at elevated temperature.

For ALD of gold metal, reactions of the alkoxide complexes with hydroborane and hydrosilane reducing agents are envisaged. These reactions could potentially proceed as shown in Scheme 1, *via* stepwise (a) precursor chemisorption to the substrate surface (likely with loss of the neutral PR_3 ligand), (b) reaction with a hydroborane or hydrosilane co-reactant to exchange the alkoxide ligand on Au with an H substituent on B or Si, forming an unstable Au–H linkage, and (c) H_2 reductive elimination from the surface to afford gold metal. Notably, step b in this process can be expected to be thermodynamically favourable due to cleavage of a hard–soft mismatched Au–O bond and formation of a very strong B–O or Si–O bond (BDEs of approx. ~500–550 kJ mol^{-1}).[30,31] Conversion of $[Au(O^tBu)(IPr)]$ (IPr = 1,3-bis(2,6-diisopropylphenyl)imidazol-2-ylidene) to $[AuH(IPr)]$ using $HSi(OMe_3)_3$ has also been reported.[32] With respect to step c, binary gold hydrides such as AuH are only stable under matrix isolation conditions or at extreme temperature and pressure,[33,34] and molecular gold(I) hydride complexes (neutral and monometallic examples) have only been stabilized by very bulky and/or highly donating carbene,[32,35,36] NHC-coordinated diphosphene (RP(NHC)–PR),[37] and phosphine[38] ligands.

Gold(I) alkoxide complexes are relatively scarce, and have been isolated with N-heterocyclic carbene (NHC),[24,32,39–42] cyclic alkylamidocarbene (CAAC),[43] phosphine,[25,39,44–47] or carbidodiphosphorane[48] neutral donors, with crystallographically characterized examples limited to $[Au(OR)(NHC)]$ (NHC = N-heterocyclic carbene; OR = O^tBu,[42] OCF_3[41] or $OCH(CF_3)_2$)[39,40] and $[Au(O^tBu)\{C(PR_3)_2\}]$ $\{C(PR_3)_2$ = a cyclic carbidodiphosphorane ligand$\}$.[48] Gold(I) thiolate complexes are far more common,[49] and were synthesized in this work to investigate the effects of softer thiolate ligands on precursor thermal stability, volatility, and reactivity.

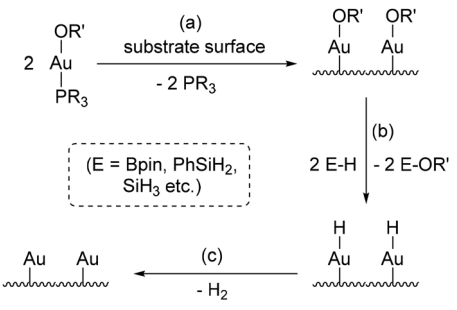

Scheme 1 Potential surface-based reactivity for gold ALD using a phosphine-coordinated gold(I) alkoxide precursor $Au\{OR'\}(PR_3)$ in combination with a hydroborane or hydrosilane co-reactant (*e.g.* HBpin, H_3SiPh or SiH_4).

Results and discussion

Reactions of the gold(I) chloro phosphine complexes AuCl(PR_3) (R = alkyl) with $NaOC(CF_3)_3$ at room temperature in CH_2Cl_2 did not proceed to a significant extent (and comparable results were obtained using AuCl(PMe_3) with $KOC(CF_3)_3$). However, in the presence of 1 equiv. of $Ag[BF_4]$ or $Ag[PF_6]$ as a halide abstraction agent, these reactions proceeded within several hours to afford the gold(I) alkoxide complexes $[(Au\{OC(CF_3)_3\}\{PR_3\})_n]$ (R = Me (**1**), Et (**2**), ^{i}Pr (**3**) and ^{t}Bu (**4**); Scheme 2(a)). Phosphine ligands were selected as the neutral donors in this work due to readily tuneable steric and electronic properties, with a focus on trialkylphosphines (rather than aryl-substituted phosphines) to maximize ligand volatility and donor ability. The steric bulk and overall electron donor ability of the phosphines in **1–4** increases in the order $PMe_3 < PEt_3 < P^iPr_3 < P^tBu_3$, with Tolman cone angles of 118, 132, 160 and 182°, respectively.[50] These phosphines also allow exploration of the potential for longer chain alkyl groups (*e.g.* R = Et *vs.* Me) to afford complexes with lower melting points.[51–63]

Compounds **1–4** were isolated in 69–89% yield as colourless solids or oils after removal of insoluble material followed by sublimation/distillation, and products arising from alkoxide transfer to silver were not observed.[64] Compounds **1–4** were characterized by ^{1}H, $^{13}C\{^1H\}$, $^{13}C\{^{19}F\}$, ^{19}F and $^{31}P\{^1H\}$ NMR spectroscopy and combustion elemental analysis, and it is notable that while the ^{19}F NMR chemical shifts are similar for all four complexes (−74.5 to −74.8 ppm), the ^{31}P NMR chemical shift varied substantially, from −19 ppm in **1**, to 26 ppm in **2**, 59 ppm in **3**, and 84 ppm in **4** (*cf.* −62 ppm, −20 ppm, 19 ppm and 61 ppm for the free phosphines).[65]

Reactions of AuCl(PR_3) with NaO^{t}Bu and AgX (X = BF_4^- or PF_6^-) were also attempted in an effort to prepare non-fluorinated analogues of **1–4**. However, the products of these reactions appear to be unstable. For example, the reaction with R and X equal to ^{i}Pr and PF_6, respectively, proceeded within 30 minutes in C_6D_6 to form a product with NMR data (see Experimental section) consistent with $[\{Au(O^tBu)(P^iPr_3)\}_n]$, but new ^{31}P NMR peaks grew in during attempts to purify the product by filtration/drying or crystallization at −33 °C. Similar results were observed for reactions using $Ag[BF_4]$ as the abstracting agent, and in both instances (reactions with $Ag[PF_6]$ or $Ag[BF_4]$), the fluorinated anion could not be completely removed from the product mixture without accompanying decomposition of the $[\{Au(O^tBu)(P^iPr_3)\}_n]$ moiety. The phosphine-coordinated gold(I) alkoxide complexes $[Au(O^tBu)(PPh_3)]$[47] and $[Au(O^tBu)(^t$Bu-xantphos$)]$[45] were also reported to decompose at room temperature in solution. As an alternative, non-fluorinated thiolate (S^tBu) analogues were pursued, to test whether these softer donors would afford more thermally stable species. The target compounds $[\{Au(S^tBu)(PR_3)\}_n]$ (R = Me (**5**) or ^{i}Pr (**6**)) were isolated as analytically pure white solids in 67 and 90% yield *via* reactions of $[\{Au(S^tBu)\}_n]$ with PR_3 (R = Me or ^{i}Pr; Scheme 2(b)), and gave rise to ^{31}P NMR chemical signals at −1 and 66 ppm, respectively. However, unlike **1–4**, they underwent complete (for **5**) or partial (for **6**) decomposition upon attempted sublimation at 5 mTorr (*vide infra*).

X-ray quality crystals of **1**, **3** and **4** were grown by slow diffusion of hexanes into concentrated CH_2Cl_2 solutions at −33 °C. In the solid state, compound **1** is a trimer (n = 3) due to aurophilic interactions (Au–Au = 3.337(1)–3.340(1) Å) which link three linear $Au\{OC(CF_3)_3\}\{PMe_3\}$ units (O–Au–P = 175.2 (1)–178.0(1)°); Fig. 2(a). Compound **1** is a relatively uncommon example of a trimer connected *via* unsupported aurophilic interactions,[66] and the Au–Au distances fall within the typical

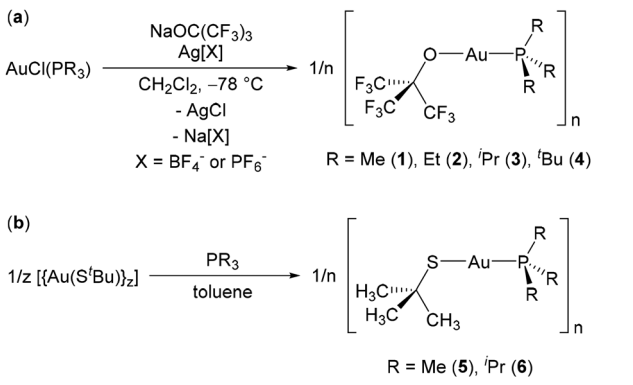

Scheme 2 Synthesis of (a) gold(I) perfluoro-*tert*-butoxide complexes **1–4** and (b) gold(I) *tert*-butylthiolate complexes **5–6**. In the solid state, trimethylphosphine compounds **1** and **5** are a trimer and a dimer, respectively, due to aurophilic interactions. Compounds **3**, **4** and **6** are monomers. The nuclearity of **2** is unknown.

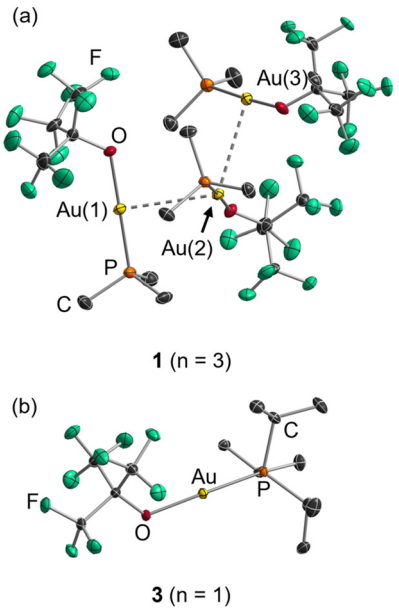

Fig. 2 X-ray crystal structures of (a) trimeric $[(Au\{OC(CF_3)_3\}\{PMe_3\})_3]$ (**1**) and (b) monomeric $[Au\{OC(CF_3)_3\}\{P^iPr_3\}]$ (**3**). In compound **1**, the CF_3 groups of the $OC(CF_3)_3$ ligands on Au(2) and Au(3) are disordered over two positions, and only the major disorder component (83.3(5)% for the ligand on Au(2), and 61.0(8)% for the ligand on Au(3)) is shown. Hydrogen atoms are omitted for clarity and thermal ellipsoids are at 50% probability.

range.[66] The Au–O distances in **1** are 2.044(3)–2.074(3) Å, placing them at the upper end of the range reported for neutral, monometallic Au-alkoxides (1.990(7)–2.061(5) Å).[40–42,48] The Au–P distances are 2.205(1)–2.220(1) Å, which are shorter than those in the respective $AuCl(PR_3)$ derivatives (2.233(3)–2.253(6) Å),[67,68] but are similar to those in other monometallic, neutral gold(I) phosphine complexes.[69] By contrast, more sterically hindered **3** (Fig. 2(b)) and **4** are linear monomers in the solid state (O–Au–P = 176.0(1) and 178.0(1)°, respectively). The Au–O distances in **3** (2.055(1) Å) and **4** (2.041(2) Å) are similar to those in **1**, whereas the Au–P distances (2.229(1) and 2.233(1) Å, respectively) are slightly longer, presumably due to increased phosphine steric bulk. Crystals of **2** were not obtained due to the low melting point of this derivative, so the solid state nuclearity of **2** is unknown. It is notable that the structure of **4** is analogous to that of the monomeric silver analogue $[Ag\{OC(CF_3)_3\}(P^tBu_3)]$, whereas the silver analogues of **1** and **3** are dimers with bridging alkoxide groups, $[(Ag\{\mu\text{-}OC(CF_3)_3\}\{PR_3\})_2]$ (R = Me or ^{i}Pr),[64] highlighting the lower preference of silver(I), *versus* gold(I), for a linear geometry.[70]

X-ray quality crystals of **5–6** were obtained by cooling hot hexanes solutions to −33 °C. Compound **5** is a dimer comprised of linear $Au(S^tBu)(PMe_3)$ units (S–Au–P = 173.1(1)–177.9(1)°) linked by aurophilic interactions (Au–Au = 3.358(1) and 3.392(1) Å); Fig. 3(a). The Au–S distances of 2.303(3)–2.310(3) Å are similar to those in $[Au(S^tBu)(PMePh_2)]$,[71] and the Au–P distances of 2.254(3)–2.266(3) Å are longer than those in **1** (and **3** and **4**), likely due to diminished electrophilicity at gold (arising from the greater electron-donor ability of S^tBu *versus* $OC(CF_3)_3$ ligands). By contrast, more sterically hindered **6** is a linear monomer (Fig. 3(b); S–Au–P = 178.3(1)°) with Au–S and Au–P distances (2.301(1) and 2.273(1) Å, respectively), similar to those in **5**.

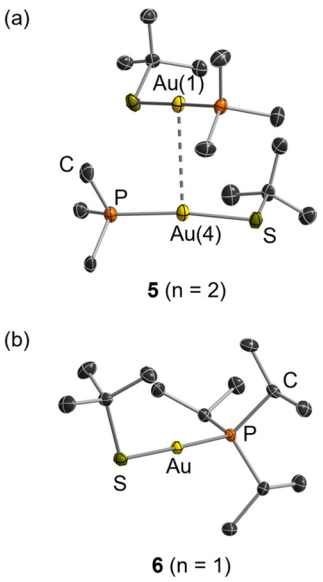

Fig. 3 X-ray crystal structures of (a) dimeric $[\{Au(S^tBu)(PMe_3)\}_2]$ (**5**) and (b) monomeric $[Au(S^tBu)(P^iPr_3)]$ (**6**). The unit cell for compound **5** contains two independent but essentially isostructural dimers, only one of which is shown. Hydrogen atoms are omitted for clarity and thermal ellipsoids are at 50% probability.

The longer Au–Au distances in **5** *versus* **1**, and the fact that **5** is a dimer whereas **1** is a trimer, is intriguing, considering the far greater steric bulk of the $OC(CF_3)_3$ ligands in **1** *versus* the S^tBu ligands in **5**. This could potentially be the result of crystal packing effects combined with the known cooperativity of aurophilic interactions, where the existence of multiple aurophilic interactions to the same metal centre increases their individual strength.[72] The increased electrophilicity (at Au) of the monomeric units in **1** could also play a role. For example, particularly short Au–Au distances in the auracarborane 1,1′-$\{Au(PPh_3)\}_2$-2,2′-(*ortho*-$C_2B_{10}H_{10})_2$ were attributed to high electron-deficiency.[73] Additionally, an experimental study of AuXL complexes (L = CN^tBu or CNMe; X = Cl, Br or I) showed stronger aurophilic interactions (shorter Au–Au distances) for the lighter more electronegative halides, resulting in lower sublimation temperatures for the iodide complexes, and similar trends were observed for phosphine analogues.[74]

For the development of new ALD methods, solution reactivity studies[12,75–77] are a valuable tool to probe (rapidly, using small amounts of material) whether a particular precursor/co-reactant combination exhibits high reactivity, as well as to determine whether this reactivity leads, in solution, to the target material (in this work, Au). They can also provide insight into fundamental reaction steps which may be relevant to the envisaged ALD process, as well as the nature and volatility of likely reaction byproducts generated during ALD. Given the envisaged ALD reactivity with hydroborane or hydrosilane co-reactants (Scheme 1), the solution reactivity of compound **1** with a slight excess (1.1 equiv. per Au) of pinacolborane (HBpin) and phenylsilane (H_3SiPh) was investigated in C_6D_6 and monitored by ^1H, ^{19}F, $^{31}P\{^1H\}$, $^{11}B\{^1H\}$ and ^1H–^{29}Si HMBC NMR spectroscopy (Fig. 4 and Fig. S42–S49).

For each reaction (**1** with HBpin and H_3SiPh), an immediate colour change occurred, from a clear colourless solution to an opaque brown-black mixture containing a fine black precipitate. NMR spectroscopy showed the formation of H_2 and free PMe_3, accompanied by (a) $\{(F_3C)_3CO\}$Bpin in the reaction with HBpin, or (b) an approximate 1 : 1 mixture of $\{(F_3C)_3CO\}SiH_2Ph$ and $\{(F_3C)_3CO\}_2SiHPh$ in the reaction with H_3SiPh. These products were identified by comparison to the literature ($\{(F_3C)_3CO\}$Bpin),[64] and by multinuclear and 2D NMR spectroscopy for $\{(F_3C)_3CO\}SiH_2Ph$ and $\{(F_3C)_3CO\}_2SiHPh$ (Fig. S46–S51). The reaction mixtures were evaporated to dryness *in vacuo* at room temperature, whereupon re-addition of C_6D_6 and NMR spectroscopy revealed near-complete removal of all reaction byproducts, indicative of appreciable volatility. The precipitates were washed with toluene, dried *in vacuo*, and identified as gold metal by PXRD (Fig. 5(a and b)). Analogous rapid reactivity was observed for **3** with HBpin and H_3SiPh. By contrast, thiolate complex **5** reacted very slowly with an excess (5 equiv.) of HBpin or H_3SiPh at room temperature (no reaction was apparent after 1 hour, and the reactions required >24 hours to reach completion).

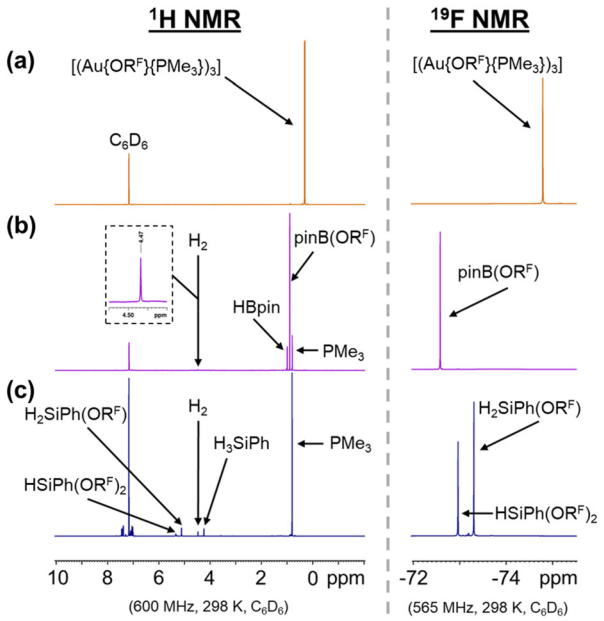

Fig. 4 ^{1}H (left) and ^{19}F (right) NMR spectra (C_6D_6, 298 K; 600 and 565 MHz, respectively) for: (a) compound **1**, (b) the reaction of **1** with 1.1 equiv. (per Au) of HBpin, and (c) the reaction of **1** with 1.1 equiv. (per Au) of H_3SiPh. OR^F = $OC(CF_3)_3$ and pin = $OCMe_2CMe_2O$.

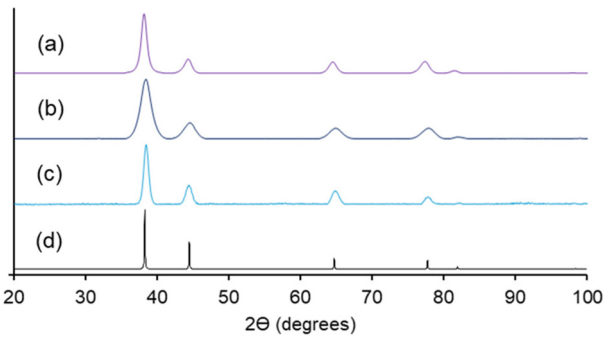

Fig. 5 Powder X-ray diffractograms (λ = 1.5406 Å) of the precipitate deposited during reactions of **1** with (a) HBpin and (b) H_3SiPh, (c) X-ray diffractogram (λ = 1.5406 Å) of a gold film deposited by sequential pulses of **3** (10 s pulses, delivered at 85 °C) and HBpin (0.03 s pulses, delivered at 8 °C) for 1000 cycles at 124 °C on a SiO_2/Si substrate (using 60 s Ar purges, and a reactor pressure of ~250 mTorr), and (d) the powder diffraction pattern for crystalline gold from the Crystallography Open Database (COD 1100138).[78] For clarity in (c), an integration mask (a wedge mask spanning 2θ = 54–59°) was applied during data processing (using Bruker DIFFRAC.EVA software) to exclude the underlying silicon substrate peak at 2θ = 56° from the diffractogram.

The potential suitability of **1–6** as CVD or ALD precursors was further assessed through comparison of sublimation (5 mTorr) temperatures and melting points, and in some cases thermogravimetric analysis (TGA), differential scanning calorimetry (DSC), and heating for days in a sealed flask under argon in the dark.

In the absence of light, perfluoro-*tert*-butoxide complexes **1–4** sublimed cleanly at 5 mTorr with minimal residue in the temperature range 50–80 °C (Table 1), and the sublimation temperature increased in the order **3** < **1** < **2** < **4**. The monomeric structure of **3** (L = P^{i}Pr$_3$) *versus* the trimeric structure of **1** (L = PMe$_3$) presumably leads to the increased volatility of **3** *versus* **1**, despite the substantially greater molecular mass of the phosphine in **3**, and the higher sublimation temperature for **4** (L = P^{t}Bu$_3$) *versus* **3** is consistent with the higher molecular mass of **4** (given that both compounds are monomers in the solid state). The higher sublimation temperature of **2** (L = PEt$_3$) *versus* **3**, despite its lower molecular mass, suggests that **2** is not a monomer. Compared to **1–4**, the thiolate complexes are less thermally stable: **5** decomposed at 80–100 °C without sublimation (5 mTorr), whereas **6** sublimed at 75–80 °C (at 5 mTorr) in the dark with partial decomposition (to provide a direct comparison between **1** and **5**, a sample of **1** was heated in the dark at 100 °C for 5 hours under dynamic vacuum at a pressure of 5 Torr (sufficient to remove free PMe$_3$, but not to volatilize **1**), resulting in negligible decomposition; Fig. S72–S74).

Table 1 Sublimation temperatures and melting points for alkoxide complexes **1–4** (X = $OC(CF_3)_3$) and thiolate complexes **5–6** (X = S^{t}Bu)

Compound [{Au(X)(PR$_3$)}$_n$]	Sublimation (5 mTorr) temperature (°C)	Melting point[a] (°C)
1 (R = Me)	55–60	105–106 (in the dark)
2 (R = Et)	65–70	19–21
3 (R = ^{i}Pr)	50–55	59–61
4 (R = ^{t}Bu)	75–80	181–183
5 (R = Me)	None (decomp. 80–100)[b]	158–160
6 (R = ^{i}Pr)	75–80 (with partial decomp.)	85–87

[a] Melting points from DSC (**1**), slowly warming a frozen drop (**2**), melting point apparatus (**3** and **6**), and DSC and melting point apparatus (**4** and **5**). Note: for **1** in a melting point apparatus (under bright light), melting is accompanied by partial decomposition with an associated colour change from colourless to pink-red. [b] Although **5** decomposed at 80–100 °C during attempted sublimation *in vacuo* (due to loss of PMe$_3$), an exothermic peak was not observed by DSC (in a sealed capsule) up to 200 °C (Fig. S37).

The insoluble residue from attempts to sublime **5** was identified as [{Au(S^{t}Bu)}$_n$] by (a) the mass of the residue, which exactly matches that expected from PMe$_3$ loss, (b) PXRD (Fig. S77 and S78), and (c) reaction of the residue with excess PMe$_3$ to cleanly re-form **5** leaving no residual solid (Fig. S76). The diminished thermal stability of the thiolate complexes relative to the alkoxide complexes may be due to weaker phosphine coordination to the less electrophilic gold centres (reflected in the longer Au–P distances in the solid state structures of **5–6** *vs.* **1** and **3–4**) combined with more favourable phosphine substitution by a soft thiolate ligand (to form a bridging thiolate ligand) compared to a hard alkoxide anion.

Given that **1–4** sublimed cleanly *in vacuo*, their volatility and thermal stability was further evaluated through thermogravimetric analysis (TGA; Fig. 6). These measurements were carried out within an inert-atmosphere glovebox at ~760 Torr, which is a far higher pressure than the previously described sublimation experiments (5 mTorr) or the operating pressure of a typical ALD reactor (*e.g.* 0.1 to 10 Torr); under these

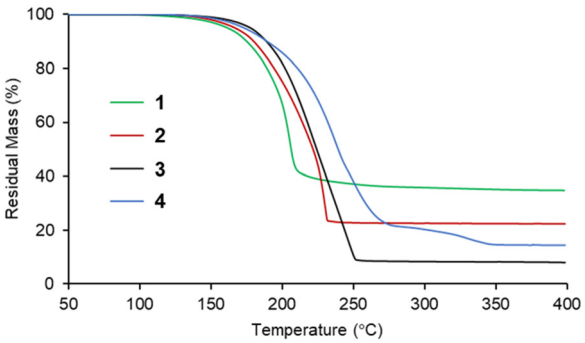

Fig. 6 Thermogravimetric analysis (TGA) mass loss curves for compounds **1–4** with a heating rate of 10 °C min^{-1} at approximately atmospheric pressure in an argon-filled glovebox. Sample masses were: **1** = 3.626 mg; **2** = 2.930 mg; **3** = 3.728 mg; **4** = 3.069 mg. The residual masses for **1–4** are 34.9, 22.4, 8.1, and 14.5%, respectively.

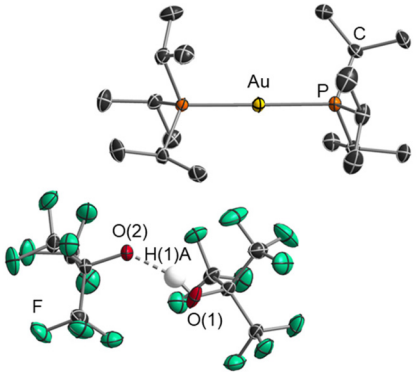

Fig. 7 X-ray crystal structure of $[Au(P^iPr_3)_2][H\{OC(CF_3)_3\}_2]$ (**7**). All hydrogen atoms except for H(1)A are omitted for clarity and thermal ellipsoids are at 50% probability. The difference Fourier map showed residual electron density between O(1) and O(2), offset towards O(1), thus an AFIX 147 command was used to place the H atom on O(1) in an idealized position, with a torsion angle chosen to locate the H atom at the position of maximum electron density.

conditions, residual masses of 34.9, 22.4, 8.1 and 14.5% were obtained for **1–4**, respectively. These residual masses are lower than the gold content of the samples (38.8, 35.8, 33.3 and 31.1 mass%, respectively), suggesting mass loss *via* combined thermal decomposition and sublimation, where compound **3** afforded the cleanest-looking TGA trace and the lowest residual mass (8.1%).

Melting points were also measured (Table 1), since CVD/ALD precursors which are liquid at the delivery temperature are desirable from a practical perspective.[13,14] The melting points for **1–4** increased in the order **2** < **3** < **1** ≪ **4**, where **2** melts at 19–21 °C, **3** melts at 59–61 °C, and **1** melts 105–106 °C. Compound **4** melted at much higher temperature (181–183 °C), but decomposed slowly at this temperature (heating a solid sample of **4** to 190 °C for 10 minutes in the absence of light led to ~6% decomposition by NMR spectroscopy).

The thermal stability of **1**, **3** and **4** was further evaluated by heating for several days in a sealed glass tube under argon at 100 °C in the absence of light or solvent (100 °C was selected because a temperature significantly higher than the 5 mTorr sublimation temperature will be required for delivery on a typical ALD reactor due to a higher operating pressure (*e.g.* ~250 mTorr for our reactors)). These reactions were carried out in the presence of approx. 1 equiv. of 4,4′-difluorobenzophenone as an internal NMR standard which contains both ^1H and ^{19}F, and is not volatile at room temperature. Under these conditions, complex **1** was ~8% decomposed after 24 hours and 100% decomposed after 96 hours. By contrast, **3** was only 3% decomposed after 24 hours at 100 °C, and ~10% decomposed after 96 hours (and comparable results were obtained in the absence of 4,4′-difluorobenzophenone). Repeating this test for **3** at 85 °C led to ~4% decomposition after 72 hours. In addition, ~3% decomposition of **4** was observed after 24 hours at 100 °C, increasing to ~11% after 96 hours.

For thermal decomposition of **3**, $[Au(P^iPr_3)_2][H\{OC(CF_3)_3\}_2]$ (**7**) was identified as the major soluble decomposition product by NMR spectroscopy and X-ray diffraction (Fig. 7), with accompanying formation of metallic gold (Fig. S71). Relative to two molecules of **3**, compound **7** contains the same number of $OC(CF_3)_3$ and P^iPr_3 groups, but one gold(I) centre has been replaced by H^+. This proton (H(1)A) is located between two oxygen centres which are 2.418(3) Å apart, and the location of the electron density in the Fourier map suggests that H(1) is primarily associated with O(1), forming an O(1)–H(1)A···O(2) hydrogen bond, although hydrogen atom locations from X-ray diffraction should be viewed with caution.[79] In the ^1H NMR spectrum of **7**, a broad singlet is observed at ~17 ppm, assigned to the proton in the $H\{OC(CF_3)_3\}_2$ anion. This chemical shift is similar to that observed for the HF_2^- anion.[80–83]

To probe whether the proton in the $[H\{OC(CF_3)_3\}_2]^-$ anion in **7** could originate from the Si–OH groups on the surface of the glass, the thermal stability of **3** was re-evaluated by heating to 100 °C for 3 days within a PTFE tube (inserted into a J-Young NMR tube) under argon. However, this test revealed a similar degree of decomposition to form **7**, suggesting that the proton must originate from a P^iPr_3 ligand. To test the feasibility of this hypothesis, a sample of **3** was heated as described above for 10 days to effect complete decomposition of **3**, and an internal standard (4,4′-difluorobenzophenone) was added in a known quantity, followed by dissolution in d_8-THF. This revealed ^1H and ^{19}F NMR integrations for **7** that are only 65% of the expected intensity (if all P^iPr_3 groups remained intact and soluble), indicating that although **7** is formed cleanly by NMR spectroscopy, it is accompanied by the formation of one or more unidentified insoluble products.

Overall, the high solution reactivity of **1** and **3** towards HBpin and H_3SiPh, forming metallic gold and volatile byproducts, highlights the potential of perfluoro-*tert*-butoxide complexes as precursors for gold thermal ALD using reducing co-reactants. Of the complexes in this work, **3** offers the best combination of thermal stability and volatility, and the relatively low melting point is attractive. Furthermore, preliminary ALD

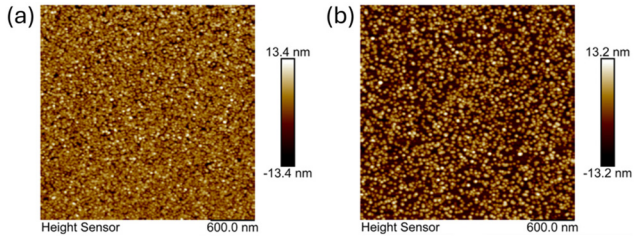

Fig. 8 AFM images of different regions of a gold film deposited on an SiO_2/Si substrate at 124 °C within an ALD reactor using 1000 cycles consisting of 10 s pulses of **3** and 0.03 s pulses of HBpin separated by 60 s purge steps. By AFM (Fig. S86), the film in location 'a' is ~15 nm thick, whereas the film in location 'b' is ~12 nm thick. These images were chosen to demonstrate the variations in particle size, particle density, and film thickness at different locations on the substrate.

reactor experiments using **3** (delivered at 85 °C) and HBpin resulted in gold deposition (identified by PXRD; Fig. 5(c)) at 124 °C, and film deposition was not observed (by AFM or XRD) at this temperature using **3** without HBpin. AFM images of this film revealed significant nanoscale non-uniformity; some regions exhibited densely packed, nearly continuous Au nanoparticle layers, whereas others showed larger particles, lower particle density and reduced local film thickness (Fig. 8 and S86). Increasing the pulse duration of **3** by 50% did not result in more uniform deposition (Fig. S87).

Non-uniform film growth could potentially be due to challenges associated with P^iPr_3 removal from the gold surface at the low deposition temperature. Incomplete removal of PMe_3 from the surface during gold ALD at 120 °C using $[AuMe_3(PMe_3)]$ and oxygen plasma was previously reported.[18] However, at higher temperature (180 °C), thermal ALD of gold was achieved without issue using the phosphine-containing precursor $[AuCl(PEt_3)]$ in combination with $\{(Me_3Ge)_2DHP\}$ (*vide supra*),[3] and gold PEALD using $[AuMe_3(PMe_3)]$ and hydrogen plasma has been reported at 50–120 °C in a reactor operating at low pressure (~5 mTorr during pulses).[17] Studies to test for self-limiting growth were not carried out due to the observed variation in film thickness across the wafer, so ALD cannot be claimed with the data that is presented. Future work will investigate $[Au\{OC(CF_3)_3\}L]$ complexes with a broader array of neutral donor ligands (L), with the goal of achieving sufficient thermal stability to allow the high reactivity of gold(I) perfluoro-*tert*-butoxide complexes to be harnessed for thermal ALD of gold using reducing co-reactants.

Summary and conclusions

This work describes the development of potential precursor molecules and reactivity for gold ALD under non-oxidizing conditions, with a focus on alkoxide complexes due to the anticipated high reactivity of the bonds between a soft gold(I) centre and a hard oxygen donor.

The gold(I) alkoxide complexes $[(Au\{OC(CF_3)_3\}\{PR_3\})_n]$ (R = Me (**1**), Et (**2**), ^{i}Pr (**3**) and ^{t}Bu (**4**)) were synthesized *via* reactions of $AuCl(PR_3)$ with $NaOC(CF_3)_3$ in the presence of 1 equiv. of Ag$[BF_4]$ or Ag$[PF_6]$, and the thiolate complexes $[\{Au(S^tBu)(PR_3)\}_n]$ (R = Me (**5**) and ^{i}Pr (**6**)) were prepared for comparison; attempts to prepare an O^{t}Bu analogue of **3** did not yield a thermally stable product. The volatility, melting points, and thermal stability of **1–6** were evaluated, and solution reactivity studies with HBpin and H_3SiPh, as well as preliminary ALD reactor studies using **3** and HBpin, were carried out. Gold(I) alkoxide complexes are relatively scarce, with only six crystallographically characterized examples prior to this work,[39–42,48] HBpin has only recently been reported as a co-reactant for metal ALD (of Cu, Bi and Ag),[64,84] and gold(I) alkoxide complexes have not previously been used as ALD precursors.

In the solid state, **1** is a trimer and **5** is a dimer due to aurophilic interactions, whereas more sterically hindered **3**, **4** and **6** are monomers. Alkoxide complex **3** underwent slow thermal decomposition at 100 °C (~10% after 96 h) to form $[Ag(P^iPr_3)_2][H\{OC(CF_3)_3\}_2]$ (**7**) accompanied by gold metal and other insoluble product(s), whereas the S^{t}Bu complex **5** decomposed over several hours at 80–100 °C to form $[\{Au(S^tBu)\}_n]$ and free PMe_3. Reactions of **1** or **3** with HBpin or H_3SiPh proceeded within seconds at room temperature to afford gold metal (accompanied by H_2, free PR_3, and either $\{(F_3C)_3CO\}$Bpin, or $\{(F_3C)_3CO\}SiH_2Ph$ and $\{(F_3C)_3CO\}_2SiHPh$), whereas analogous reactions with thiolate complex **5** required >24 hours to reach completion. Preliminary ALD reactivity studies using **3** and HBpin afforded gold thin films at 124 °C.

These findings highlight the value of strongly electron-withdrawing $OC(CF_3)_3$ ligands to obtain gold(I) phosphine complexes which are (a) less prone to decomposition *via* phosphine dissociation than O^{t}Bu or S^{t}Bu analogues, likely due to higher electrophilicity at gold, combined with less favourable phosphine substitution by a hard alkoxide ligand compared with a soft thiolate ligand (to form a bridging alkoxide or thiolate ligand), and (b) far more reactive towards hydrosilanes and hydroboranes than their thiolate (S^{t}Bu) counterparts due to the high reactivity of the hard–soft mismatched Au–O bond, and the formation of a very strong B–O or Si–O bond (rather than a B–S or Si–S bond). Variation of the phosphines also provided access to complexes with low melting points (*e.g.* approx. 20 °C for **2** and 60 °C for **3**), which is beneficial from a practical perspective: precursors which are liquid at the ALD delivery temperature minimize issues with particulate formation, delivery system blockages due to sublimation, and evaporation rate variation caused by changes in average particle size and/or concentration of impurities on the solid surface as the precursor is consumed.

The solid state structures of **1** and **3–6** reveal the influence of ligand selection on the presence/strength of aurophilic interactions, which significantly influence the volatility of the complexes. Longer Au–P distances in the thiolate *versus* the alkoxide complexes (despite substantially reduced steric hindrance) also confirm weaker phosphine coordination to the less electrophilic gold centres in the former, which is reflected in the thermal behaviour of the thiolate *vs.* alkoxide complexes (**5** decomposed much more rapidly than **1** or **3**, *via* phosphine dissociation).

Isolation/identification of products formed in solution reactions with hydroboranes and hydrosilanes, and from thermal decomposition studies, provides insight into the types of reaction that may be operative during ALD or CVD. Furthermore, preliminary ALD reactor experiments using **3** with HBpin support the viability of gold(I) [$(Au\{OC(CF_3)_3\}L)_n$] complexes for metal ALD, providing impetus for future studies exploring a broader array of neutral donors (L) to further increase the thermal stability and/or volatility of this class of complexes, so that their high reactivity can be harnessed for ALD.

Experimental

General methods

An argon-filled MBraun UNIlab or Innovative Technology PureLab HE glove box equipped with a −33 °C freezer was employed for the manipulation and storage of all air-sensitive compounds, and reactions were performed on a double manifold vacuum line using standard techniques.[85] The vacuum was measured periodically using a Kurt J. Lesker 275i convection-enhanced Pirani gauge. Residual oxygen and moisture were removed from the argon stream by passage through an Oxisorb-W scrubber from Matheson Gas Products. Centrifugation was carried out using a Benchmark Hermle Z206A centrifuge housed within a glove box. Note: syntheses of **1–4** using $Ag[PF_6]$ proceeded more rapidly and slightly more cleanly than those using $Ag[BF_4]$. However, the lower-solubility $Na[BF_4]$ byproduct from reactions with $Ag[BF_4]$ was more completely removed by filtration or centrifugation.

Dichloromethane, diethyl ether, hexanes, tetrahydrofuran, and toluene were purchased from Sigma-Aldrich, deuterated solvents (C_6D_6 or d_8-THF) were purchased from Cambridge Isotope Laboratories. These solvents were initially dried and distilled at atmospheric pressure from sodium/benzophenone (deuterated benzene, diethyl ether, hexanes, tetrahydrofuran), sodium (toluene), or 4 Å molecular sieves (dichloromethane). All dried solvents were stored over sodium/benzophenone except for dichloromethane, which was stored over 4 Å molecular sieves. Ethanol and methanol were purchased from Sigma-Aldrich; ethanol was used as purchased, whereas methanol was dried and stored over 4 Å molecular sieves. Dry solvents were introduced to reactions or solvent storage flasks *via* vacuum transfer with condensation at −78 °C.

Trimethylphosphine, triethylphosphine and tri-*tert*-butylphosphine were purchased from Strem Chemicals; the former two were transferred to a solvent storage flask under inert conditions, and the latter was stored in a −33 °C freezer in an Ar-filled glovebox. Chlorodiisopropylphosphine (P^iPr_2Cl) was obtained from Sigma-Aldrich or Thermo Fisher Scientific, dried over 4 Å molecular sieves and distilled into a storage flask. Magnesium powder was obtained from Merck KGaA and stored in an Ar-filled glovebox. Perfluoro-*tert*-butanol (HOC$(CF_3)_3$) was obtained from Oakwood Chemical and dried over 4 Å molecular sieves prior to distillation into a storage flask. Hexafluoroacetylacetone (hfacH), 2-chloropropane and tetrahydrothiophene (THT) were obtained from Sigma-Aldrich. Sodium hydride (NaH) was obtained from Sigma-Aldrich and stored in an Ar-filled glovebox. Silver tetrafluoroborate and silver hexafluorophosphate were obtained from Sigma-Aldrich and stored under inert conditions in the absence of light. *tert*-Butylthiol was obtained from Oakwood Chemical. Gold(III) chloride hydrate ($HAuCl_4{\cdot}xH_2O$; 48% Au content by weight) was obtained from AmBeed Inc.

Other starting materials were synthesized *via* literature procedures, or slight modifications of these procedures. AuCl(THT) was prepared by treatment of $HAuCl_4{\cdot}xH_2O$ with excess tetrahydrothiophene (THT) in a 5 : 1 mixture of ethanol and water.[18] Triisopropylphosphine (P^iPr_3) was prepared by addition of isopropylmagnesium chloride (freshly prepared by sonicating a stoichiometric amount of magnesium powder suspended in Et_2O for 10 minutes, followed by addition of 2-chloropropane and gentle heating to 35 °C for approximately 2 hours with continuous stirring) to a solution containing one equivalent of chlorodiisopropylphosphine in Et_2O at 0 °C. This was allowed to warm to room temperature and stir overnight, whereupon the reaction mixture was distilled at reduced pressure and the solvent removed at −78 °C under reduced pressure. $^{31}P\{^1H\}$ NMR (C_6D_6, 242 MHz, 298 K): 19.4 ppm.[86] AuCl(PR_3) (R = Me, Et, ^{i}Pr) starting materials were prepared by treatment of AuCl(THT) with one equivalent of the corresponding phosphine in dichloromethane.[18] AuCl(P^tBu_3) was prepared by direct treatment of $HAuCl_4{\cdot}xH_2O$ with excess P^tBu_3 in dry methanol.[87] Sodium perfluoro-*tert*-butoxide ($NaOC(CF_3)_3$) and sodium hexafluoroacetylacetonate (Na(hfac)) were prepared by deprotonation of perfluoro-*tert*-butanol (HOC$(CF_3)_3$) and hexafluoroacetylacetone (hfacH), respectively, with sodium hydride in THF.[88–90] Polymeric Au(S^tBu) was prepared by treatment of $HAuCl_4{\cdot}xH_2O$ with excess *tert*-butylthiol (HS^tBu) in a 4 : 1 mixture of methanol and water.[91]

NMR spectroscopy was performed on a Bruker AV-600 spectrometer. All ^1H NMR and ^{13}C NMR spectra were referenced relative to $SiMe_4$ through the C_6D_6 or d_8-THF resonance or the protio impurity in the C_6D_6 and d_8-THF: 7.16 and 3.58 ppm, respectively, for ^1H NMR and 128.06 and 67.21 ppm, respectively, for ^{13}C NMR. ^{19}F, ^{31}P and ^{11}B NMR spectra were referenced to $CFCl_3$ (Ξ = 94.094011%), 85% aqueous H_3PO_4 (Ξ = 40.480742%), and $BF_3(OEt_2)$ (Ξ = 32.083974%), respectively, by indirect referencing from a ^1H NMR spectrum.[92] Peak assignments in the spectra of all new diamagnetic compounds were made with the aid of HSQC and HMBC experiments. NMR chemical shift abbreviations: s = singlet, d = doublet, t = triplet, q = quartet, sept. = septet, m = multiplet, app. = apparent, br. = broad, virt. = virtual.

Single-crystal X-ray crystallographic analyses were performed on crystals coated in Paratone oil and mounted on either a STOE IPDS II diffractometer with an image plate detector, or a Bruker Dual Source D8 Venture diffractometer using the IμS 3.0 Mo source at 70 W with a HELIOS Mo focusing optic (ELM33) in the McMaster Analytical X-ray (MAX) Diffraction Facility. Raw data was processed using XPREP

(as part of the APEX v2/4/5 software) and solved by intrinsic phasing (SHELXT).[93] In all cases, non-hydrogen atoms were refined anisotropically. Hydrogen atoms were generated in ideal positions and then updated with each cycle of refinement, which was performed with SHELXL in OLEX2-1.5.[94,95]

Powder X-ray diffraction (PXRD) and thin film X-ray diffraction (XRD) was carried out on a Bruker Dual Source D8 Venture diffractometer equipped with a PHOTON CMOS (Complementary Metal Oxide Semiconductor) area detector and an Incoatec IμS Cu source (Kα radiation; λ = 1.54184 Å), operated at 50 kV and 1.10 mA in the MAX Diffraction Facility.

Combustion elemental analyses were performed by Midwest Microlabs in Indianapolis, Indiana or at the University of Calgary using a PerkinElmer Model 2400 series II analyzer. Thermogravimetric analysis was performed by Green Centre Canada (now Impact Chemistry), in Kingston, Ontario using a TA Instruments Discovery TGA located within an argon-filled glove box. Melting point determinations were performed by packing the analyte into a flame-sealed pipette and sealing the open face of the pipette with Apiezon H-grease inside an argon-filled glovebox. The pipette was then removed from the glovebox and quickly flame-sealed (below the grease but sufficiently distant from the analyte) to form a sealed capillary, which was in turn used for analysis using a DigiMelt Melting Point Apparatus.

Atomic force microscopy (AFM) imaging was performed at the McMaster Centre for Advanced Light Microscopy (CALM) facility using a Bruker Dimension iCon AFM equipped with a Bruker TESPA-V2 probe, operated in tapping mode. AFM data analysis was performed using Bruker NanoScope Analysis 3.00.

The ALD reactor used for preliminary studies has previously been described.[96] However, in this work, the oven surrounding the ALD reaction chamber was heated to 100 °C, and argon flows of 20 sccm were used on each of the four inlet lines, affording a reactor pressure of ~250 mTorr during deposition. Compound **3** was contained in a flow-through delivery vessel maintained at 85 °C, while HBpin was in a non-flow-through delivery vessel maintained at 8 °C by immersing it in a beaker of water on a thermoelectric cooling plate. The experiment used 10 s pulses of **3**, 0.03 s pulses of HBpin, 60 s purges, 1000 cycles, and a substrate temperature of 124 °C. Attempted CVD using 10 s pulses of **3** (without any co-reactant, using 1000 pulses separated by 60 s purges) at 124 °C did not result in any film growth. Long purge durations (*e.g.* 60 s) are required on this ALD reactor due to a large reactor volume (the heated substrate stage is located within a 4.5″ Conflat cube).

[(Au{OC(CF$_3$)$_3$}{PMe$_3$})$_3$] (1)

167 mg (0.54 mmol) of AuCl(PMe$_3$), 141 mg (0.54 mmol) of NaOC(CF$_3$)$_3$, and 106 mg (0.54 mmol) of Ag[BF$_4$] were added to a 50 mL flask wrapped in foil. The flask was cooled to −78 °C, whereupon 15 mL of CH_2Cl_2 was introduced *via* vacuum distillation. The resulting solution was warmed to room temperature over the course of ~30 minutes, and the reaction was stirred for an additional 4 hours. The solution was evaporated to dryness *in vacuo*, and the resulting solid was redissolved in toluene. Insoluble material was removed by centrifugation, and the supernatant solution was evaporated to dryness *in vacuo* to yield analytically pure **1** (245 mg, 0.16 mmol, 89%) as a white, crystalline solid. The product can be sublimed *in vacuo* (5 mTorr) at 60 °C in the absence of light, leaving minimal residue. Crystals suitable for single crystal X-ray diffraction (SCXRD) were grown by vapour diffusion of hexanes into a concentrated CH_2Cl_2 solution at −33 °C. ^{1}H NMR (C_6D_6, 600 MHz, 298 K): δ 0.31 (d, P(CH_3)$_3$, $^2J_{HP}$ = 12 Hz). ^{13}C{^{1}H} NMR (C_6D_6, 151 MHz, 298 K): δ 123.92 (q, *C*F$_3$, $^1J_{CF}$ = 294 Hz); 84.39 (*C*(CF$_3$)$_3$);† 14.52 (d, P(*C*H$_3$)$_3$, $^1J_{CP}$ = 43 Hz). ^{19}F NMR (C_6D_6, 565 MHz, 298 K): δ −74.78 (s, C*F*$_3$). ^{31}P{^{1}H} NMR (C_6D_6, 243 MHz, 298 K): δ −18.95 (s, *P*Me$_3$). Melting point: 105–106 °C by DSC (note: in a melting point apparatus, under bright illumination, melting was accompanied by partial decomposition). Anal. calcd for $C_{21}H_{27}Au_3F_{27}O_3P_3$ (%): C, 16.55; H, 1.79. Found: C, 16.81; H, 1.81. Note: a reaction of AuCl(PMe$_3$) with 3 eq. K_2CO_3 and 2 eq. HOC(CF$_3$)$_3$ in EtOH (in air) was also attempted, following methods developed for the synthesis of [M(OC{R}{CF$_3$}$_2$)(L)] (M = Cu[97–99] (R = CF$_3$ or H, L = NHC) or Au[39,40] (R = H and L = NHC or PR$_3$)) complexes. This reaction was stirred for 24 hours, followed by evaporation to dryness *in vacuo*, and redissolution in CD_2Cl_2. However, ^{31}P{^{1}H} NMR spectroscopy showed a mixture of remaining AuCl(PMe$_3$) (49%), two unidentified species (^{31}P δ 7.3 and −17.8 ppm; 19 and 23%, respectively), and only a small amount of **1** (9%).

[(Au{OC(CF$_3$)$_3$}{PEt$_3$})$_n$] (2)

Compound **2** was prepared analogously to **1** using 320 mg (0.91 mmol) of AuCl(PEt$_3$), 235 mg (0.91 mmol) of NaOC(CF$_3$)$_3$, 177 mg (0.91 mmol) of Ag[BF$_4$], and 20 mL of CH_2Cl_2. After evaporation of the reaction solution, a waxy solid was obtained, centrifugation in toluene and evaporation to dryness afforded an amber oil, and distillation *in vacuo* (5 mTorr) at 70 °C afforded **2** (360 mg, 0.65 mmol, 71%) as a colourless, low melting solid (which begins to melt upon handling at room temperature). ^{1}H NMR (C_6D_6, 600 MHz, 298 K): δ 0.74 (br s, 6H, P(CH_2CH$_3$)$_3$), 0.51 (br s, 9H, P(CH$_2$CH_3)$_3$). ^{13}C{^{1}H} NMR (C_6D_6, 151 MHz, 298 K): δ 124.10 (*q*, *C*F$_3$, $^1J_{CF}$ = 295 Hz); 84.83 (*C*(CF$_3$)$_3$);‡ 17.54 (d, P(*C*H$_2$CH$_3$)$_3$, $^1J_{CP}$ = 37 Hz); 8.77 (s, P(CH$_2$*C*H$_3$)$_3$). ^{19}F NMR (C_6D_6, 565 MHz, 298 K): δ −74.75 (s, C*F*$_3$). ^{31}P{^{1}H} NMR (C_6D_6, 243 MHz, 298 K): δ 25.66 (s, *P*Et$_3$). Melting point: 19–21 °C. Anal. calcd for $C_{10}H_{15}AuF_9OP$ (%): C, 21.83; H, 2.75. Found: C, 22.09; H, 2.83.

[Au{OC(CF$_3$)$_3$}(P^{i}Pr$_3$)] (3)

Compound **3** was prepared analogously to **1** using 247 mg (0.62 mmol) of AuCl(P^{i}Pr$_3$), 160 mg (0.62 mmol) of NaOC(CF$_3$)$_3$, 120 mg (0.62 mmol) of Ag[BF$_4$], and 15 mL of CH_2Cl_2. After evaporation of the reaction solution, a waxy solid was

† Located as a singlet by ^{13}C{^{19}F} NMR spectroscopy.
‡ Peak identified/confirmed by the presence of a cross peak in the ^{13}C–^{19}F HMBC NMR spectrum.

obtained, centrifugation in toluene and evaporation to dryness afforded an off-white solid, and pure **3** (274 mg, 0.46 mmol, 74%) was obtained as a colourless crystalline solid by recrystallization from a 3 : 1 mixture of hexanes and toluene at −33 °C. The product can be sublimed *in vacuo* (5 mTorr) at 50–55 °C in the absence of light, leaving minimal residue. Crystals suitable for SCXRD were grown by vapour diffusion of hexanes into a concentrated CH_2Cl_2 solution at −33 °C. ^{1}H NMR (C_6D_6, 600 MHz, 298 K): δ 1.30 (d sept., 3H, P(C*H*$(CH_3)_2)_3$, $^2J_{HP}$ = 9 Hz, $^3J_{HH}$ = 7 Hz), 0.62 (dd, 18H, P(CH(C$H_3)_2)_3$, $^3J_{HP}$ = 16 Hz, $^3J_{HH}$ = 7 Hz). ^{13}C{^{1}H} NMR (C_6D_6, 151 MHz, 298 K): δ 124.04 (q, *C*F_3, $^1J_{CF}$ = 295 Hz); 84.51 (*C*$(CF_3)_3$);[†,‡] 23.27 (d, P(*C*H$(CH_3)_2)_3$, $^1J_{CP}$ = 34 Hz); 19.70 (s, P(CH(*C*$H_3)_2)_3$). ^{19}F NMR (C_6D_6, 565 MHz, 298 K): δ −74.64 (s, C*F*$_3$). ^{31}P{^{1}H} NMR (C_6D_6, 243 MHz, 298 K): δ 58.52 (s, *P*^{i}Pr$_3$). Melting point: 59–61 °C. Anal. calcd for $C_{13}H_{21}AuF_9OP$ (%): C, 26.36; H, 3.58. Found: C, 26.59; H, 3.97.

[Au{OC(CF$_3$)$_3$}(P^{t}Bu$_3$)] (4)

Compound **4** was prepared analogously to **1** using 79 mg (0.18 mmol) of AuCl(P^{t}Bu$_3$), 46 mg (0.18 mmol) of NaOC$(CF_3)_3$, 35 mg (0.18 mmol) of Ag[BF_4], and 10 mL of CH_2Cl_2 in a 25 mL flask. After evaporation of the reaction solution, a pinkish off-white solid was obtained, centrifugation in toluene and evaporation to dryness afforded an off-white solid, and pure **4** (79 mg, 0.12 mmol, 69%) was obtained as a colourless crystalline solid by recrystallization from a 3 : 1 mixture of hexanes and toluene at −33 °C. The product can be sublimed *in vacuo* (5 mTorr) at 75–80 °C in the absence of light, leaving minimal residue. Crystals suitable for SCXRD were grown by vapour diffusion of hexanes into a concentrated CH_2Cl_2 solution at −33 °C. ^{1}H NMR (C_6D_6, 600 MHz, 298 K): δ 0.91 (d, P(C(C$H_3)_3)_3$, $^3J_{HP}$ = 14 Hz). ^{13}C{^{1}H} NMR (C_6D_6, 151 MHz, 298 K): δ 124.09 (q, *C*F_3, $^1J_{CF}$ = 293 Hz); 84.61 (*C*$(CF_3)_3$);† 38.62 (d, P(*C*$(CH_3)_3)_3$, $^1J_{CP}$ = 23 Hz); 31.60 (s, P(C(C$H_3)_3)_3$). ^{19}F NMR (C_6D_6, 565 MHz, 298 K): δ −74.53 (s, C*F*$_3$). ^{31}P{^{1}H} NMR (C_6D_6, 243 MHz, 298 K): δ 84.12 (s, *P*^{t}Bu$_3$). Melting point: 181–183 °C. Anal. calcd for $C_{16}H_{27}AuF_9OP$ (%): C, 30.29; H, 4.30. Found: C, 30.28; H, 4.37.

[{Au(S^{t}Bu)(PMe$_3$)}$_2$] (5)

Polymeric Au(S^{t}Bu) (83 mg; 0.29 mmol) was suspended in 6 mL of toluene in a 25 mL flask, and 30 μL (22 mg, 0.29 mmol) of PMe_3 was added under a flow of dynamic argon. The reaction mixture was stirred at room temperature for 2 hours and evaporated to dryness *in vacuo*. The resulting solid was redissolved in toluene, insoluble material was removed by centrifugation, and the supernatant was evaporated to dryness *in vacuo* to yield **5** (103 mg, 0.13 mmol, 90% yield) as an analytically pure white powder. Crystals suitable for SCXRD were grown by dissolving **5** in hot hexanes, followed by cooling the solution to −33 °C. ^{1}H NMR (C_6D_6, 600 MHz, 298 K): δ 1.93 (s, 9H, SC(C$H_3)_3$); 0.48 (d, 9H, P(C$H_3)_3$, $^2J_{HP}$ = 10 Hz). ^{13}C{^{1}H} NMR (C_6D_6, 151 MHz, 298 K): δ 44.21 (s, SC$(CH_3)_3$); 40.54 (s, SC(*C*$H_3)_3$); 14.96 (d, P(*C*$H_3)_3$, $^1J_{CP}$ = 34 Hz). ^{31}P{^{1}H} NMR (C_6D_6, 243 MHz, 298 K): δ −0.51 (s, *P*Me_3). Melting point: 158–160 °C within a sealed tube/capsule which prevents loss of PMe_3 (attempted vacuum sublimation resulted in decomposition to form phosphine-free [{Au(S^{t}Bu)}$_n$] at 80–100 °C). Anal. calcd for $C_{14}H_{36}Au_2S_2P_2$ (%): C, 23.21; H, 5.02. Found: C, 23.61; H, 5.29.

[Au(S^{t}Bu)(P^{i}Pr$_3$)] (6)

Compound **6** was prepared analogously to **5** using 129 mg of Au(S^{t}Bu) (0.45 mmol), 86 μL (72 mg, 0.45 mmol) of P^{i}Pr$_3$, and 6 mL of toluene. The resulting white solid (after centrifugation in toluene and evaporation to dryness) was washed with hexanes and dried *in vacuo* to yield **6** (134 mg, 0.30 mmol, 67% yield) as an analytically pure white powder. Crystals suitable for SCXRD were grown by dissolving **6** in hot hexanes, followed by cooling the solution to −33 °C. ^{1}H NMR (C_6D_6, 600 MHz, 298 K): δ 1.94 (s, 9H, SC(C$H_3)_3$); 1.57 (app. octet, 3H, P(C*H*$(CH_3)_2)_3$, $J \sim 8$ Hz), 0.81 (dd, 18H, P(CH(C$H_3)_2)_3$, $^3J_{HP}$ = 7 Hz, $^3J_{HH}$ = 8 Hz). ^{13}C{^{1}H} NMR (C_6D_6, 151 MHz, 298 K): δ 44.16 (s, SC$(CH_3)_3$); 40.68 (s, SC(*C*$H_3)_3$); 23.65 (d, P(*C*H$(CH_3)_2)_3$, $^1J_{CP}$ = 26 Hz); 19.95 (s, P(CH(*C*$H_3)_2)_3$). ^{31}P{^{1}H} NMR (C_6D_6, 243 MHz, 298 K): δ 66.44 (s, *P*^{i}Pr$_3$). Melting Point: 85–87 °C within a sealed tube (note: attempted sublimation at 5 mTorr led to a mixture of sublimation and decomposition at 75–80 °C). Anal. calcd for $C_{13}H_{30}AuSP$ (%): C, 34.97; H, 6.79. Found: C, 34.84; H, 7.02.

In situ synthesis of [{Au(O^{t}Bu)(P^{i}Pr$_3$)}$_n$]

11 mg (0.03 mmol) of Au(Cl)(P^{i}Pr$_3$) was dissolved in 500 mg C_6D_6 in an NMR tube, and 3 mg (0.03 mmol) of NaO^{t}Bu and 7 mg (0.03 mmol) of Ag[PF_6] were added. The tube was shaken and sonicated for approximately 5 minutes, whereupon the solution took on a translucent, beige colour. NMR spectroscopy was conducted approximately 30 minutes after addition, affording peaks consistent with a stoichiometric product of [{Au(O^{t}Bu)(P^{i}Pr$_3$)}$_n$]. A PF_6-containing moiety was also present in solution in an approximately 3 : 1 ratio with the P^{i}Pr$_3$ signal. ^{1}H NMR (C_6D_6, 600 MHz, 298 K): δ 1.66 (s, 9H, OC(C$H_3)_3$); 1.60 (app. octet, 3H, P(C*H*$(CH_3)_2)_3$, $J \sim 8$ Hz), 0.88 (dd, 18H, P(CH(C$H_3)_2)_3$, $^3J_{HP}$ = 7 Hz, $^3J_{HH}$ = 8 Hz). ^{13}C{^{1}H} NMR (C_6D_6, 151 MHz, 298 K): δ 72.27 (s, O*C*$(CH_3)_3$); 37.01 (s, OC(*C*$H_3)_3$); 23.44 (d, P(*C*H$(CH_3)_2)_3$, $^1J_{CP}$ = 32 Hz); 20.00 (s, P(CH(*C*$H_3)_2)_3$). ^{31}P{^{1}H} NMR (C_6D_6, 242 MHz, 298 K): δ 56.51 (s, 3P, *P*^{i}Pr$_3$), −142.82 (sept., 1P, *P*F_6, $^1J_{PF}$ = 713 Hz). Attempts to isolate the [{Au(O^{t}Bu)(P^{i}Pr$_3$)}$_n$] product from this reaction, as well as repeat reactions on a larger scale, were unsuccessful.

Thermal stability tests for [Au{OC(CF$_3$)$_3$}(PR$_3$)] (R = Me (1), ^{i}Pr (3) or ^{t}Bu (4))

Long-term thermal stability tests were conducted by obtaining NMR spectra (^{1}H, ^{19}F, in C_6D_6) of the precursor of interest and an internal standard (4,4′-difluorobenzophenone) in a J-Young NMR tube to serve as a baseline. The solvent was then removed *in vacuo*, and the dried solids were placed under 1 atm of argon. The sample was wrapped in aluminium foil and placed in an oil bath which had been heated to the target

temperature. The tube was left at this temperature for a given time, following which the tube was cooled in the absence of light, the contents were redissolved in C_6D_6, and NMR spectra were acquired. Integration of the precursor and decomposition product peaks relative to the internal standard yielded approximate decomposition percentages. Comparable results (based on integration of starting material and product peaks) were obtained carrying out the thermal decomposition of **3** at 100 °C in the absence of the internal standard.

Thermal decomposition of 3 to form $[Au(P^iPr_3)_2][H\{OC(CF_3)_3\}_2]$ (7)

In all instances regarding the thermal decomposition of **3**, one major soluble product (**7**) was identified by NMR spectroscopy. **Method A**: to obtain crystals of **7** suitable for SCXRD, 26 mg of **3** was added to a 50 mL Schlenk flask and sealed under 1 atm of argon. The flask was heated to 100 °C in the dark for 96 hours, and the contents of the flask were extracted with 2 × 3 mL portions of toluene and centrifuged. The toluene solution was concentrated and placed into a −30 °C freezer to yield colourless crystals of **3** and **7**. The residual solids were dried *in vacuo* and PXRD was performed, showing broad peaks for metallic gold accompanied by sharper peaks due primarily to **3** and **7** (the latter of which is only sparingly soluble in toluene) (Fig. S71). **Method B**: a sample of **3** was completely decomposed by heating as described above for 10 days, whereupon **7** was identified as the major soluble product by NMR spectroscopy, with trace signals (<3%) attributed to an unknown product with $^{31}P\{^1H\}$ NMR δ = 62.85 (C_6D_6, 243 MHz, 298 K) (Fig. S70). NMR spectroscopic data for **7**: ^1H NMR (C_6D_6, 600 MHz, 298 K): $\delta \sim 17$ ppm (br s, 1 H, $H\{OC(CF_3)_3\}_2$), 1.85 (sept. virt. t, 6H, $P(CH(CH_3)_2)_3$, $^2J_{HP} \sim 7$ Hz,§ $^3J_{HH} = 7$ Hz); 0.89 (d virt. t, 36H, $P(CH(CH_3)_2)_3$, $^3J_{HP} \sim 16$ Hz,§ $^3J_{HH} = 7$ Hz). $^{13}C\{^1H\}$ NMR (C_6D_6, 151 MHz, 298 K): δ 82.03‡ ($H\{OC(CF_3)_3\}_2$), 23.76 (virt. t, $^2J_{CP} = 28$ Hz,§ $P(CH(CH_3)_2)_3$), 23.38 (s, $P(CH(CH_3)_2)_3$); the CF_3 peak was not observed in the $^{13}C\{^1H\}$ NMR spectrum, but was located in the $^{13}C\{^{19}F\}$ NMR spectrum as a singlet at 123.88 ppm. ^{19}F NMR (C_6D_6, 565 MHz, 298 K) δ −73.82 (s, $H\{OC(CF_3)_3\}_2$). $^{31}P\{^1H\}$ NMR (C_6D_6, 243 MHz, 298 K): δ 75.62 (s, P^iPr_3).¶ ^1H NMR (d_8-THF, 600 MHz, 298 K): $\delta \sim 16.5$ ppm (br s, 1 H, $H\{OC(CF_3)_3\}_2$), 2.64 (sept. virt. t, 6H, $P(CH(CH_3)_2)_3$, $^2J_{HP} \sim 7$ Hz,§ $^3J_{HH} = 7$ Hz); 0.89 (d virt. t, 36H, $P(CH(CH_3)_2)_3$, $^3J_{HP} \sim 16$ Hz,§ $^3J_{HH} = 7$ Hz). ^{19}F NMR (d_8-THF, 565 MHz, 298 K) δ −75.22 (s, $H\{OC(CF_3)_3\}_2$). $^{31}P\{^1H\}$ NMR (d_8-THF, 243 MHz, 298 K): δ 76.16 (s, P^iPr_3).¶

X-ray crystal Structure of $[Au(\kappa^1C\text{-hfac})(P^iPr_3)]$

This compound was prepared analogously to **1** using 106 mg (0.27 mmol) of $AuCl(P^iPr_3)$, 61 mg (0.27 mmol) of Na(hfac), 52 mg (0.27 mmol) of $Ag[BF_4]$, and 10 mL of CH_2Cl_2 in a 25 mL flask. After evaporation of the reaction solution, a purplish off-white solid was obtained. Soluble products were dissolved in toluene, the mixture was centrifuged, and the filtrate was evaporated to dryness to afford a waxy orange oil. This oil was sonicated for 5 minutes (until it dissolved) in 5 mL of hexanes, and the solution was evaporated to dryness *in vacuo* to yield a white, waxy solid. A pure bulk sample of this complex was not obtained due to an apparent lack of thermal stability, but X-ray quality crystals were obtained by layering a toluene solution with hexanes in a 1 : 2 ratio and cooling to −33 °C.

§ The signal contains a virtual triplet arising from an AA′X spin system. The apparent coupling constant (observed) for the triplet is the average of J_{AX} and $J_{A'X}$, where $J_{AX} = 0$ Hz.

¶ Similar ^{31}P chemical shifts were observed for $[Au(P^iPr_3)_2][Cl]$[100] and $[Au(P^iPr_3)_2][BF_4]$.[101]

Conflicts of interest

There are no conflicts to declare.

Data availability

Data supporting this article is included in the supplementary information (SI). Supplementary information: selected NMR spectra, X-ray diffraction, TGA and DSC data, and AFM images. See DOI: https://doi.org/10.1039/d5dt02836a.

CCDC 2503049–2503054 and 2505331 for **1**, **3**–**7**, and $[Au(\kappa^1C\text{-hfac})(P^iPr_3)]$ contain the supplementary crystallographic data for this paper.[102a–g]

Acknowledgements

D. J. H. E. thanks NSERC of Canada for a Discovery Grant, and the Ontario government for an Ontario Research Fund Research Excellence (ORF-RE) grant. N. A. H. thanks NSERC of Canada for CGS-M and PGS-D awards, and the Ontario government for an OGS award. The authors thank Prof. Yurij Mozharivskyj for access to his X-ray diffractometer, Prof. Alex Adronov for access to his DSC instrument, the McMaster Analytical X-ray (MAX) Diffraction Facility, the McMaster Centre for Advanced Light Microscopy (CALM), and Dr Jeffrey Price for helpful crystallographic discussions.

References

1 D. R. Lide, in *CRC Handbook of Chemistry and Physics*, CRC Press. Taylor & Francis Group, Boca Raton, FL, 87 edn, 2006, ch. 12.
2 J. P. Mendes, P. S. S. dos Santos, B. Dias, S. Núñez-Sánchez, I. Pastoriza-Santos, J. Pérez-Juste, C. M. Pereira, P. A. S. Jorge, J. de Almeida and L. C. C. Coelho, *Adv. Opt. Mater.*, 2024, **12**, 2400433.
3 A. Vihervaara, T. Hatanpää, H.-E. Nieminen, K. Mizohata, M. Chundak and M. Ritala, *ACS Mater. Au*, 2023, **3**, 206–214.
4 S. Z. Liang, M. Schwartzkopf, S. V. Roth and P. Müller-Buschbaum, *Nanoscale Adv.*, 2022, **4**, 2533–2560.

5 T. V. Basova, A. Hassan and N. B. Morozova, *Coord. Chem. Rev.*, 2019, **380**, 58–82.
6 S. Lal, S. Link and N. J. Halas, *Nat. Photonics*, 2007, **1**, 641–648.
7 G. Popov, M. Mattinen, A. Vihervaara and M. Leskelä, *J. Vac. Sci. Technol., A*, 2025, **43**, 030801.
8 R. W. Johnson, A. Hultqvist and S. F. Bent, *Mater. Today*, 2014, **17**, 236–246.
9 D. J. Hagen, M. E. Pemble and M. Karppinen, *Appl. Phys. Rev.*, 2019, **6**, 041309.
10 V. Miikkulainen, M. Leskelä, M. Ritala and R. L. Puurunen, *J. Appl. Phys.*, 2013, **113**, 021301.
11 T. J. Knisley, L. C. Kalutarage and C. H. Winter, *Coord. Chem. Rev.*, 2013, **257**, 3222–3231.
12 D. J. H. Emslie, P. Chadha and J. S. Price, *Coord. Chem. Rev.*, 2013, **257**, 3282–3296.
13 N. A. Hoffman and D. J. H. Emslie, *Can. J. Chem.*, 2024, **102**, 620–628.
14 S. E. Koponen, P. G. Gordon and S. T. Barry, *Polyhedron*, 2016, **108**, 59–66.
15 M. Mäkelä, T. Hatanpää, K. Mizohata, J. Räisänen, M. Ritala and M. Leskelä, *Chem. Mater.*, 2017, **29**, 6130–6136.
16 R. G. Parkhomenko, I. K. Igumenov, S. E. Hadjadj, S. V. Trubin and M. Knez, *Nanoscale*, 2025, **17**, 2318–2325.
17 M. Van Daele, M. B. E. Griffiths, A. Raza, M. M. Minjauw, E. Solano, J.-Y. Feng, R. K. Ramachandran, S. Clemmen, R. Baets, S. T. Barry, C. Detavernier and J. Dendooven, *ACS Appl. Mater. Interfaces*, 2019, **11**, 37229–37238.
18 M. B. E. Griffiths, P. J. Pallister, D. J. Mandia and S. T. Barry, *Chem. Mater.*, 2016, **28**, 44–46.
19 M. Mäkelä, T. Hatanpää, M. Ritala, M. Leskelä, K. Mizohata, K. Meinander and J. Räisänen, *J. Vac. Sci. Technol., A*, 2017, **35**, 01B112.
20 F. S. M. Hashemi, F. Grillo, V. R. Ravikumar, D. Benz, A. Shekhar, M. B. E. Griffiths, S. T. Barry and J. R. van Ommen, *Nanoscale*, 2020, **12**, 9005–9013.
21 E. R. T. Tiekink, *Acta Crystallogr., Sect. C:Cryst. Struct. Commun.*, 1989, **45**, 1233–1234.
22 D. R. Boris, V. D. Wheeler, N. Nepal, S. B. Qadri, S. G. Walton and C. R. Eddy, *J. Vac. Sci. Technol., A*, 2020, **38**, 040801.
23 H. B. Profijt, S. E. Potts, M. C. M. van de Sanden and W. M. M. Kessels, *J. Vac. Sci. Technol., A*, 2011, **29**, 050801.
24 D. S. Laitar, P. Müller, T. G. Gray and J. P. Sadighi, *Organometallics*, 2005, **24**, 4503–4505.
25 Y. Usui, J. Noma, M. Hirano and S. Komiya, *Inorg. Chim. Acta*, 2000, **309**, 151–154.
26 R. G. Pearson, *J. Am. Chem. Soc.*, 1963, **85**, 3533–3539.
27 K. I. Grandberg, L. G. Kuz'mina, E. I. Smyslova, A. I. Zinin, D. P. Krut'ko and V. P. Dyadchenko, *Zh. Neorg. Khim.*, 1996, **41**, 231–239.
28 L. G. Kuz'mina, *Koord. Khim.*, 1994, **20**, 540–546.
29 D. Gibson, B. F. G. Johnson and J. Lewis, *J. Chem. Soc. A*, 1970, 367–369.
30 N. J. Mosey, K. M. Baines and T. K. Woo, *J. Am. Chem. Soc.*, 2002, **124**, 13306–13321.
31 M. Sana, G. Leroy and C. Wilante, *Organometallics*, 1992, **11**, 781–787.
32 E. Y. Tsui, P. Müller and J. P. Sadighi, *Angew. Chem., Int. Ed.*, 2008, **47**, 8937–8940.
33 M. Frost, K. Abraham, A. F. Goncharov, R. S. McWilliams, R. J. Husband, M. Andrzejewski, K. Appel, C. Baehtz, A. Bergermann, D. Brown, E. Bykova, A. Celeste, E. Edmund, N. J. Hartley, K. Glazyrin, H. Graafsma, N. Jaisle, Z. Konôpková, T. Laurus, Y. Lin, B. Massani, M. Schörner, M. Schulze, C. Strohm, M. Tang, Z. Younes, G. Steinle-Neumann, R. Redmer and S. H. Glenzer, *Angew. Chem., Int. Ed.*, 2025, **64**, e202505811, and references therein.
34 K. T. Nguyen, V. Vuong, T. N. Nguyen, T. T. Nguyen, T. Yamamoto and N. N. Hoang, *Nat. Commun.*, 2021, **12**, 1560.
35 T. L. Zhou, P. C. Gao, R. Lalancette, R. Szostak and M. Szostak, *Nat. Chem.*, 2024, **16**, 2025–2035.
36 N. Phillips, T. Dodson, R. Tirfoin, J. I. Bates and S. Aldridge, *Chem. – Eur. J.*, 2014, **20**, 16721–16731.
37 D. Dhara, S. Das, S. K. Pati, D. Scheschkewitz, V. Chandrasekhar and A. Jana, *Angew. Chem., Int. Ed.*, 2019, **58**, 15367–15371.
38 M. Navarro, M. Holzapfel and J. Campos, *Inorg. Chem.*, 2023, **62**, 10582–10591.
39 P. Arnaut, N. B. Pozsoni, F. Nahra, N. V. Tzouras and S. P. Nolan, *Dalton Trans.*, 2024, **53**, 11952–11958.
40 N. V. Tzouras, A. Gobbo, N. B. Pozsoni, S. G. Chalkidis, S. Bhandary, K. Van Hecke, G. C. Vougioukalakis and S. P. Nolan, *Chem. Commun.*, 2022, **58**, 8516–8519.
41 C. P. Zhang and D. A. Vicic, *Organometallics*, 2012, **31**, 7812–7815.
42 M. T. Johnson, J. M. J. van Rensburg, M. Axelsson, M. S. G. Ahlquist and O. F. Wendt, *Chem. Sci.*, 2011, **2**, 2373–2377.
43 A. S. Romanov and M. Bochmann, *Organometallics*, 2015, **34**, 2439–2454.
44 F. J. L. Ingner, Z. X. Giustra, S. Novosedlik, A. Orthaber, P. J. Gates, C. Dyrager and L. T. Pilarski, *Green Chem.*, 2020, **22**, 5648–5655.
45 J. Y. Hu, J. Zhang, G. X. Wang, H. L. Sun and J. L. Zhang, *Inorg. Chem.*, 2016, **55**, 2274–2283.
46 S. Komiya, M. Iwata, T. Sone and A. Fukuoka, *J. Chem. Soc., Chem. Commun.*, 1992, 1109–1110.
47 B. R. Sutherland, K. Folting, W. E. Streib, D. M. Ho, J. C. Huffman and K. G. Caulton, *J. Am. Chem. Soc.*, 1987, **109**, 3489–3490.
48 R. Corberán, S. Marrot, N. Dellus, N. Merceron-Saffon, T. Kato, E. Peris and A. Baceiredo, *Organometallics*, 2009, **28**, 326–330.
49 I. O. Koshevoy, E. S. Smirnova, M. Haukka, A. Laguna, J. C. Chueca, T. A. Pakkanen, S. P. Tunik, I. Ospino and O. Crespo, *Dalton Trans.*, 2011, **40**, 7412–7422, and references therein.

50 C. A. Tolman, *Chem. Rev.*, 1977, **77**, 313–348.
51 R. Samii, S. C. Buttera, V. Kessler and N. J. O'Brien, *Eur. J. Inorg. Chem.*, 2022, **2022**, e202200161.
52 M. Gakiya-Teruya, X. Jiang, D. Le, Ö. Üngör, A. J. Durrani, J. J. Koptur-Palenchar, J. Jiang, T. Jiang, M. W. Meisel, H.-P. Cheng, X.-G. Zhang, X.-X. Zhang, T. S. Rahman, A. F. Hebard and M. Shatruk, *J. Am. Chem. Soc.*, 2021, **143**, 14563–14572.
53 N. S. Nikolaeva, N. V. Kuratieva, E. S. Vikulova, P. A. Stabnikov and N. B. Morozova, *Polyhedron*, 2019, **171**, 455–463.
54 N. Harmgarth, P. Liebing, L. Hilfert, V. Lorenz, F. Engelhardt, S. Busse and F. T. Edelmann, *Z. Anorg. Allg. Chem.*, 2019, **645**, 1101–1109.
55 K. Soussi, S. Mishra, E. Jeanneau, A. Mantoux and S. Daniele, *Polyhedron*, 2018, **152**, 84–89.
56 K. Lubitz, V. Sharma, S. Shukla, J. H. J. Berthel, H. Schneider, C. Hoßbach and U. Radius, *Organometallics*, 2018, **37**, 1181–1191.
57 K. I. Karakovskaya, E. S. Vikulova, D. A. Piryazev and N. B. Morozova, *J. Struct. Chem.*, 2017, **58**, 1427–1431.
58 J. Masnovi, N. V. Duffy, P. E. Fanwick and A. F. Hepp, *J. Coord. Chem.*, 2016, **69**, 90–102.
59 M. Krasnopolski, C. G. Hrib, R. W. Seidel, M. Winter, H.-W. Becker, D. Rogalla, R. A. Fischer, F. T. Edelmann and A. Devi, *Inorg. Chem.*, 2013, **52**, 286–296.
60 T. Chen, C. Xu, T. H. Baum, G. T. Stauf, J. F. Roeder, A. G. DiPasquale and A. L. Rheingold, *Chem. Mater.*, 2010, **22**, 27–35.
61 M. Eleter, S. Daniele, V. Brize, C. Dubourdieu, C. Lachaud, N. Blasco and A. Pinchart, *ECS Trans.*, 2009, **25**, 151–158.
62 A. Baunemann, M. Lemberger, A. J. Bauer, H. Parala and R. A. Fischer, *Chem. Vap. Deposition*, 2007, **13**, 77–83.
63 K.-H. Park and W. J. Marshall, *J. Am. Chem. Soc.*, 2005, **127**, 9330–9331.
64 N. A. Hoffman and D. J. H. Emslie, *Chem. Mater.*, 2026, accepted.
65 J. C. Tebby, *CRC Handbook of Phosphorus-31 Nuclear Magnetic Resonance Data*, CRC Press, Taylor & Francis Group, Boca Raton, FL, 1991.
66 H. Schmidbaur and A. Schier, *Chem. Soc. Rev.*, 2012, **41**, 370–412.
67 K. Angermaier, E. Zeller and H. Schmidbaur, *J. Organomet. Chem.*, 1994, **472**, 371–376.
68 H. Schmidbaur, B. Brachthäuser, O. Steigelmann and H. Beruda, *Chem. Ber.*, 1992, **125**, 2705–2710.
69 92 instances of neutral $AuX(PR_3)$ (R = Me, ^{i}Pr or ^{t}Bu; X = any monodentate anionic ligand; R and X are not bridging ligands) complexes were found on the CSD, with Au–P distances ranging from 2.204 to 2.352 Å; CSD accessed via Conquest (CSD version 6.00, updated April, 2025).
70 M. A. Carvajal, J. J. Novoa and S. Alvarez, *J. Am. Chem. Soc.*, 2004, **126**, 1465–1477.
71 A. Battisti, O. Bellina, P. Diversi, S. Losi, F. Marchetti and P. Zanello, *Eur. J. Inorg. Chem.*, 2007, **2007**, 865–875.
72 J. M. Guevara-Vela, K. Hess, T. Rocha-Rinza, A. M. Pendás, M. Flores-Álamo and G. Moreno-Alcántar, *Chem. Commun.*, 2022, **58**, 1398–1401.
73 D. E. Harwell, M. D. Mortimer, C. B. Knobler, F. A. L. Anet and M. F. Hawthorne, *J. Am. Chem. Soc.*, 1996, **118**, 2679–2685.
74 W. G. Carden, J. Pedziwiatr, K. A. Abboud and L. McElwee-White, *ACS Appl. Mater. Interfaces*, 2017, **9**, 40998–41005.
75 B. Vidjayacoumar, D. J. H. Emslie, J. M. Blackwell, S. B. Clendenning and J. F. Britten, *Chem. Mater.*, 2010, **22**, 4854–4866.
76 B. Vidjayacoumar, D. J. H. Emslie, S. B. Clendenning, J. M. Blackwell, J. F. Britten and A. Rheingold, *Chem. Mater.*, 2010, **22**, 4844–4853.
77 B. Vidjayacoumar, V. Ramalingam, D. J. H. Emslie, J. Blackwell and S. Clendenning, *ECS Trans.*, 2013, **50**, 53–66.
78 J. Spreadborough and J. W. Christian, *J. Sci. Instrum.*, 1959, **36**, 116–118.
79 P. Müller, in *Crystal Structure Refinement: A Crystallographer's Guide to SHELXL*, ed. P. Müller, R. Herbst-Irmer, A. L. Spek, T. R. Schneider and M. R. Sawaya, Oxford University Press, 2006, pp. 26–41.
80 J. Soriano, J. Shamir, A. Netzer and Y. Marcus, *Inorg. Nucl. Chem. Lett.*, 1969, **5**, 209–214.
81 P. Schah-Mohammedi, I. G. Shenderovich, C. Detering, H.-H. Limbach, P. M. Tolstoy, S. N. Smirnov, G. S. Denisov and N. S. Golubev, *J. Am. Chem. Soc.*, 2000, **122**, 12878–12879.
82 N. S. Golubev, S. M. Melikova, D. Shchepkin, I. G. Shenderovich, P. M. Tolstoy and G. S. Denisov, *Z. Phys. Chem.*, 2003, **217**, 1549–1564.
83 H. J. Han, J. H. Oh, J. L. Sessler and S. K. Kim, *Chem. Commun.*, 2019, **55**, 10876–10879.
84 A. Vihervaara, T. Hatanpää, K. Mizohata, M. Chundak and M. Ritala, *ACS Omega*, 2025, **10**, 51760–51766.
85 B. J. Burger and J. E. Bercaw, in *Experimental Organometallic Chemistry*, American Chemical Society, 1987, vol. 357, ch. 4, pp. 79–115.
86 W. Voskuil and J. F. Arens, *Org. Synth.*, 1968, **48**, 47.
87 H. Schmidbaur and A. A. M. Aly, *Z. Naturforsch. B*, 1979, **34**, 23–26.
88 R. E. A. Dear, W. B. Fox, R. J. Fredericks, E. E. Gilbert and D. K. Huggins, *Inorg. Chem.*, 1970, **9**, 2590–2591.
89 R. J. De Pasquale, *J. Org. Chem.*, 1973, **38**, 3025–3030.
90 Y. Harada and G. S. Girolami, *Polyhedron*, 2007, **26**, 1758–1762.
91 V. P. Dyadchenko, N. M. Belov, M. A. Dyadchenko, Y. L. Slovokhotov, A. M. Banaru and D. A. Lemenovskii, *Russ. Chem. Bull.*, 2010, **59**, 539–543.
92 R. K. Harris, E. D. Becker, S. M. C. de Menezes, R. Goodfellow and P. Granger, *Pure Appl. Chem.*, 2001, **73**, 1795–1818.
93 G. Sheldrick, *Acta Crystallogr., Sect. A: Found. Adv.*, 2015, **71**, 3–8.
94 O. V. Dolomanov, L. J. Bourhis, R. J. Gildea, J. A. K. Howard and H. Puschmann, *J. Appl. Crystallogr.*, 2009, **42**, 339–341.

95 G. Sheldrick, *Acta Crystallogr., Sect. C:Struct. Chem.*, 2015, **71**, 3–8.
96 M. Al Hareri and D. J. H. Emslie, *Chem. Mater.*, 2022, **34**, 2400–2409.
97 T. Ruggiero, K. Van Hecke, C. S. J. Cazin and S. P. Nolan, *Dalton Trans.*, 2025, **54**, 1329–1333.
98 S. Ostrowska, G. Carì, A. Czapik, M. Kwit, C. S. J. Cazin and S. P. Nolan, *Eur. J. Inorg. Chem.*, 2025, **28**, e202400740.
99 S. Ostrowska, P. Arnaut, D. J. Liptrot, C. S. J. Cazin and S. P. Nolan, *Chem. Commun.*, 2023, **59**, 9126–9129.
100 H. Ehlich, A. Schier and H. Schmidbaur, *Organometallics*, 2002, **21**, 2400–2406.
101 Y. Miyamoto, S. Aggarwal, J. J. A. Celaje, S. Ihara, J. Ang, D. B. Eremin, K. M. Land, L. A. Wrischnik, L. Zhang, V. V. Fokin and L. Eckmann, *J. Med. Chem.*, 2021, **64**, 6608–6620.
102 (*a*) CCDC 2503049: Experimental Crystal Structure Determination, 2025, DOI: 10.5517/ccdc.csd.cc2q0mjx; (*b*) CCDC 2503050: Experimental Crystal Structure Determination, 2025, DOI: 10.5517/ccdc.csd.cc2q0mky; (*c*) CCDC 2503051: Experimental Crystal Structure Determination, 2025, DOI: 10.5517/ccdc.csd.cc2q0mlz; (*d*) CCDC 2503052: Experimental Crystal Structure Determination, 2025, DOI: 10.5517/ccdc.csd.cc2q0mm0; (*e*) CCDC 2503053: Experimental Crystal Structure Determination, 2025, DOI: 10.5517/ccdc.csd.cc2q0mn1; (*f*) CCDC 2503054: Experimental Crystal Structure Determination, 2025, DOI: 10.5517/ccdc.csd.cc2q0mp2; (*g*) CCDC 2505331: Experimental Crystal Structure Determination, 2025, DOI: 10.5517/ccdc.csd.cc2q3040.